remote sensing

MDPI

Technical Note

The Use of High-Resolution Satellite Imagery to Determine the Status of a Large-Scale Outbreak of Southern Pine Beetle

Michael K. Crosby [1,*], T. Eric McConnell [2], Jason J. Holderieath [3], James R. Meeker [4], Chris A. Steiner [4], Brian L. Strom [4] and Crawford (Wood) Johnson [4]

1 School of Agricultural Sciences and Forestry, Louisiana Tech University, Ruston, LA 71272, USA
2 Department of Forestry, Mississippi State University, Starkville, MS 39762, USA; eric.mcconnell@msstate.edu
3 School of Agricultural Sciences, Northwest Missouri State University, Maryville, MO 64468, USA; jholderieath@nwmissouri.edu
4 Forest Health Protection, United States Forest Service, Pineville, LA 71360, USA; james.meeker@usda.gov (J.R.M.); chris.steiner@usda.gov (C.A.S.); brian.strom@usda.gov (B.L.S.); wood.johnson@usda.gov (C.J.)
* Correspondence: mcrosby@latech.edu

Abstract: Timely detection of insect infestation (or other disturbance) in a forest is vital for an adequate response plan to be developed. To determine the status of an active infestation of southern pine beetle (*Dendroctonus frontalis*) in the Bienville National Forest, WorldView-2 imagery was utilized. Principal components analysis (PCA) was performed and correlated with spectral reflectance bands to assess differences between the classification of spectral reflectance bands and principal components. Unsupervised classification of combinations of principal components (e.g., combining principal components 1 and 2, principal component 1 alone, and principal component 2 alone) was performed and compared with combinations of principal component correlations with spectral reflectance bands (e.g., all bands, bands 1–5, bands 6–8, and bands 2, 4, and 5). Combining principal components 1 and 2 was more accurate than other methods, closely followed by spectral bands 1–5. Employing PCA will aid resource managers in quickly detecting areas of active insect infestation and allow them to deploy adequate response measures to prevent or mitigate continued outbreaks.

Keywords: bark beetles; southern pine beetle; *Dendroctonus frontalis*; WorldView-2; principal components analysis; forest disturbance

check for updates

Citation: Crosby, M.K.; McConnell, T.E.; Holderieath, J.J.; Meeker, J.R.; Steiner, C.A.; Strom, B.L.; Johnson, C. The Use of High-Resolution Satellite Imagery to Determine the Status of a Large-Scale Outbreak of Southern Pine Beetle. *Remote Sens.* **2024**, *16*, 582. https://doi.org/10.3390/rs16030582

Academic Editor: Nicholas Coops

Received: 18 December 2023
Revised: 19 January 2024
Accepted: 1 February 2024
Published: 3 February 2024

1. Introduction

Southern pine is an essential component of the world's wood fiber production, with 18% of the global pulp and paper output coming from forests in the 13 southern states [1]. The region is also a producer of dimensional lumber products and energy production in the form of wood pellets distributed globally, and the forest plays a role in biodiversity and ecosystem services [2,3]. Pine is the predominantly planted species in the region, the majority of which is loblolly pine (*Pinus taeda* L.) [2]. Roundwood production on pine plantations accounts for 74% of pulp production in the region [3]. Given this level of production, many southern U.S. states rely on the forest industry as a significant contributor to state and local economies. Active forest landowners (the majority of the land in this region is privately owned) often seek to manage their land to maximize biomass production or use the income received to fund other non-timber related goals. The southern pine beetle (*Dendroctonus frontalis* Zimmermann; SPB) is a key disruptor to achieving those objectives as one of the most destructive forest insects in the southeastern United States. Over $40 million (USD) in damage is attributed to SPB each year [4]. Multiple generations of SPB can be hatched in a year, overwhelming trees and spreading throughout a forest. In these extreme instances, multi-year outbreaks can occur, producing waves of losses in pine forests. In terms of mitigation, management is the best policy with thinning and prescribed fire reducing the impacts of SPB in a forest [5].

Insect monitoring and detection efforts help to determine counts and insect sex ratios that may preclude an outbreak [6,7]. Once started, SPB outbreaks can be difficult to manage. Typically, a buffer is created around trees identified as being infested, and healthy trees within the buffer are directionally felled in the hopes of containing the spread [8]. One issue when working to contain an infestation or outbreak is the early detection of SPB presence. Field crews working from the ground can typically neither visit enough locations to adequately determine SPB presence nor determine if apparently healthy green trees may be infested, meaning that when trees are cut to mitigate spread, SPB may already be outside the containment area.

Detecting infested trees/areas over a large area (e.g., a national forest) is important for the timely allocation of resources to treat the area to mitigate further spread. Using remote sensing methods to detect SPB infestation and damage began with incorporating aerial photographs into monitoring efforts. The aerial photographs were utilized and work was performed to identify optimal spectral regions for identifying damaged trees [9]. Identification of damage extent and SPB presence has more recently been accomplished using satellite data, encompassing the use of spectral bands, vegetation indices, manual interpretation, image classification methods, and change detection to determine SPB presence, damage extent, and severity [10–13]. Using spectral and thermal data, it was found that canopy temperatures are impacted by early attacks by insects and could be important for monitoring and modeling early impacts of insects [14]. Detection of insect infestation or damage improves with increased spatial or temporal resolution as greater temporal resolution allows for the examination of spectral signatures over finer time frames and a greater spatial resolution allows for the analysis of individual tree crowns. Using multi-date imagery was found to provide a greater likelihood of detecting intermediate damage [11] and a greater spatial resolution allows for infested trees and portions of stands to be digitized for the development of treatment protocols [11,12,15,16].

It is now possible to utilize high-resolution imagery to provide forest managers with accurate information regarding disturbance in forests [17]. To facilitate the use of high-resolution imagery for operational and management actions it is necessary to identify rapidly deployable methodologies for image analysis that accurately identifies SPB infestation. Detection of disturbance from insects early in the process allows for the production of infestation maps and more reliable projections of how an infestation might spread to nearby trees. Using high-resolution data, the identification of early impacts, and the green-attack stage of insect infestation, is possible [18]. As with other studies, image indices using infrared portions of the electromagnetic spectrum proved the most useful as these bands (i.e., SWIR and NIR) are most closely associated with vegetation water content and health [10–15,17]. Using WorldView-2 imagery, it was found that using vegetation indices complemented insect and disease surveys conducted in situ as the satellite coverage allowed for assessment in areas it was difficult for field crews to reach [12]. Image classification with high-resolution imagery is also utilized with supervised classification methods yielding accuracy between 85–90% [17,19]. Unmanned aerial vehicles were also employed with multi-spectral cameras used to calculate image indices to detect early stress in forests [20].

Operationally, resource managers need a way to quickly and accurately determine changes in forest health conditions. Therefore, it is imperative to determine SPB activity as quickly as possible in order to manage and contain SPB activity. In the case of an outbreak, finding all impacted areas can help guide ground surveys and personnel tasked with treatment (tree felling, etc.). Using moderate-resolution imagery and image indices or classification techniques can help identify infestation in the red attack stage [10]. Using moderate-resolution sensors, such as Landsat, is dependent upon the temporal resolution of the satellite pass. Supervised classification techniques require the acquisition of training datasets to train classifiers, while on-demand methods such as unmanned aerial vehicles often have shorter flight durations not conducive to assessing large areas. Higher-resolution imagery is capable of detecting portions of single-tree canopies in multiple spectral bands; this, however, makes classification more computationally intensive. Principal component analysis (PCA) can reduce multiple bands into fewer bands, with most of the variance in a multi-band image being accounted for in the first few principal components (PCs; [21,22]). Classifying the PCs can increase the accuracy of classifications by eliminating redundant spectral information. Previous work with high-resolution imagery has utilized supervised classification techniques [12] and/or derived image indices [18] to assess mortality or infestation spread.

There is a need to provide forest managers with a way to leverage imagery to determine the current status of the forest. Rapid monitoring, evaluation, and prediction will become increasingly crucial as SPB is projected to continue moving further north as global temperatures increase [23,24]. The current research seeks to pursue that means by leveraging WorldView-2 (WV2) data to compare combinations of spectral bands and classification techniques to determine which most accurately identifies a large-scale infestation by SPB. There is the potential for confusion in assessing disturbance, particularly insect outbreaks, when considering ongoing response efforts. In cases where trees are felled in response to SPB attack (e.g., cut-and-leave), the senescing trees can appear as those currently infested. The classifications will be assessed by performing PCA on the imagery to minimize the number of spectral bands used in classification to produce a map of the current state of the forest in a humid-subtropical pine forest.

2. Materials and Methods

The Bienville National Forest (BNF) covers approximately 81,000 hectares of federal land and is located in central Mississippi in the southeastern United States (Figure 1). The climate of the region is humid-subtropical with an average annual temperature of approximately 18.5 °C and 1600 mm of precipitation distributed throughout the year. The BNF is dominated by planted pine forests (*Pinus* spp.) and the proclamation area is interspersed with privately-owned land, much of which has pine forest present. The public portions of the BNF are managed by the U.S. Forest Service and consist of planted and natural stands of approximately 63,000 ha suitable for timber production. Much of the forest is loblolly pine (*Pinus taeda*) which is difficult to transition to other forest types because of the presence of red-cockaded woodpeckers (https://www.fs.usda.gov/main/mississippi/landmanagement/planning (accessed 6 December 2023). A previous SPB outbreak impacted the forest in 2012 [5] with the most recent outbreak beginning in 2015. The spread of SPB in the BNF led to various treatment efforts in an attempt to control the outbreak [16]. These efforts include cut-and-leave, where trees are cut in a circular buffer around the infested trees to cover an area that is at least the height of the tallest infested tree. Also employed are cut-and-remove operations where trees are cut and removed to processing facilities and hazard mitigation cuts where infested and/or previously killed trees along rights-of-ways are removed. Through 2017, cut-and-leave was the primary operation for mitigating SPB spread but field-based monitoring proved difficult to keep up with SPB spots.

Worldview-2 imagery was selected to assess the outbreak given its availability of eight spectral bands, including five visible (i.e., coastal blue (400–450 nm), blue (450–510 nm), green (510–580 nm), yellow (585–625 nm), and red (630–690 nm)), red-edge (705–745 nm), and two near-infrared bands (NIR, 770–895 nm and 860–1040 nm, for NIR bands 1 and 2, respectively), and those with a high temporal resolution, and a spatial resolution of approximately two meters. Ideally, tree-level classification can be made using object-based classification methods. In the present effort, we seek to provide a reliable spectral classification of trees likely affected by SPB to better allocate field-based resources and mitigation or treatment efforts for future outbreaks. The imagery was obtained on 24 October 2017 and consisted of 12 tiled images. The tiles were converted to top-of-atmosphere radiance ([12]; Equation (1)):

$$\mathrm{L} = \mathrm{GAIN} \times \mathrm{DN} \times \left(\frac{\mathrm{abscalfactor}}{\mathrm{effectivebandwidth}}\right) \times \mathrm{OFFSET} \tag{1}$$

where L = top-of-atmosphere radiance (W/µm/m^2/sr); GAIN and OFFSET are the calibration factors provided for each spectral band; DN represents the digital number in the original image; 'abscalfactor' is the absolute calibration factor; and 'effectivebandwidth' is the effective band width (provided in the image metadata).

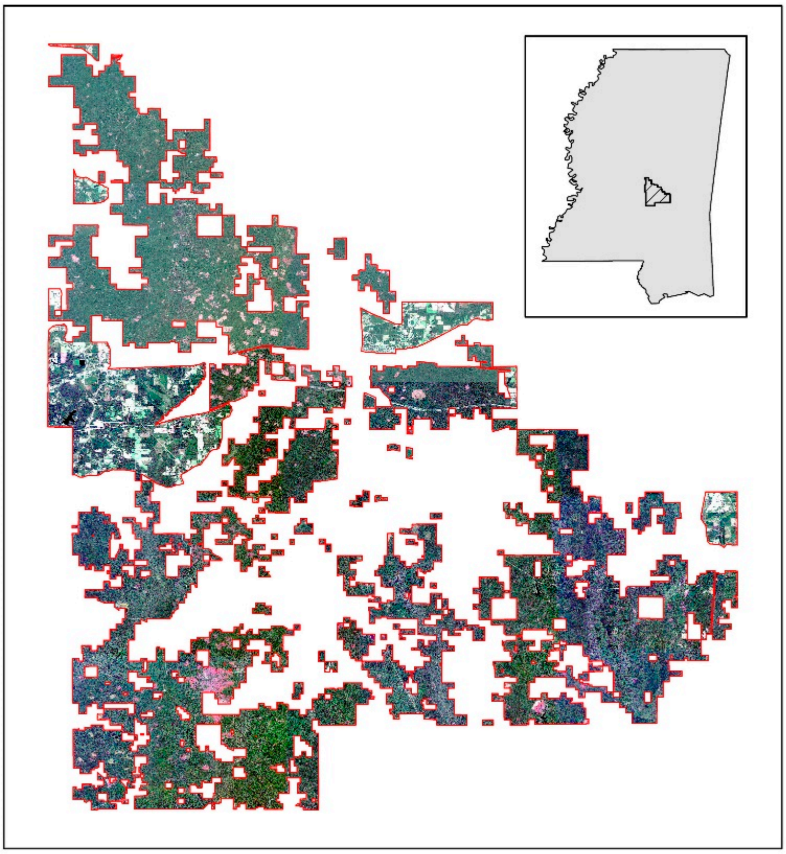

Figure 1. WorldView-2 image of federal lands within the Bienville National Forest in central Mississippi, USA.

The radiance values (L) are converted to top-of-atmosphere reflectance (Equation (2)):

$$\mathrm{TOA} = \left(\frac{\mathrm{L} \times \mathrm{dist}^2 \times \pi}{\mathrm{Esun} \times \cos\theta}\right) \tag{2}$$

where TOA = top-of-atmosphere reflectance, L = radiance (Equation (1)), dist = distance to the Sun (in astronomical units) on the date of image acquisition, Esun = top-of-atmosphere solar radiation for each band, and Θ = solar zenith angle for time/date of acquisition.

Subsequent to this, rapid atmospheric correction was applied using ERDAS Imagine 2020 [25]. This compensates for light scatter and absorption as energy propagates through the atmosphere, reducing TOA reflectance to ground-level reflectance. The tiles were mosaicked into a single image covering the public lands of Bienville.

Principal components analysis is a data reduction technique that produces orthogonal transformations of the data that produce fewer dimensions by accounting for interrelated variables [21]. PCA with remote sensing data utilizes the spectral bands of the original image and calculates a covariance matrix. Eigenvalues are derived that provide insights into the direction and magnitude of the correlation of each band to each principal component generated and can be utilized to determine the total and cumulative variance of each principal component. Principal components (PCs) are uncorrelated images that reduce data redundancy and when visualized individually or as a multiband image can elucidate underlying factors related to potential issues on the ground [18,26]. The output is a number of PCs that equal the number of input bands (i.e., eight input bands result in eight PCs). The PCs account for variance in the bands of the input image and typically capture a high proportion of the variance in the first few PCs. It is possible to analyze band correlations with each PC to assess the information captured in each component.

The PCA results were used to classify SPB infestation and to create image stacks of the band combinations accounting for the most variance in the image for classification. A principal component was calculated for each input band (8 total). Using the eigenvalues, it was observed that approximately 88% of the variance was accounted for by PC_1 and 98% of the variance in PC_1 and PC_2 (Table 1). Assessing the correlation of each band and PC, the strongest correlations for PC_1 occur with bands 6, 7, and 8 (red edge, NIR1, and NIR2, respectively). The second PC had strong negative correlations with bands 1–5 with the strongest in blue, yellow, and red bands (bands 2, 4, and 5; Table 2). Ultimately, it was decided to create images of (1) all bands, (2) coastal blue, blue, green, yellow, and red, (3) red edge, NIR1, and NIR2, and (4) blue, yellow, and red for classification. A new image was created for each combination and unsupervised classification was performed on each image. Object classifications were performed for PC_1 and PC_2 separately and a combination of PC_1 and PC_2 using an unsupervised classification. Unsupervised classification using the ISODATA clustering algorithm was employed as it provides a means of quickly assigning a class label and avoids the added costs and time of obtaining training datasets. The initial classifications divided each image into 150 clusters. Following the initial classifications, each image was reclassified as infested or non-infested by manually evaluating the initial clusters. For the object classifications using the PC results, the images were segmented, using the default segmentation parameters, and classified into 150 objects which were then reclassified into infested/non-infested objects. All classifications were performed using ArcGIS Pro version 2.8 [27].

Table 1. Principal component results showing variance and cumulative variance for each principal component.

Principal Component	% Total Variance	Cumulative Variance
1	88.2	88.2
2	9.7	97.9
3	1.0	99
4	0.5	99.5
5	0.3	99.8
6	0.1	99.9
7	0.06	99.96
8	0.04	100

To assess the accuracy of the classifications, 75 points were allocated to the infested and non-infested classes (150 points total) using an equalized stratified random distribution. Each point was then manually interpreted from the WorldView-2 image as infested or non-infested. The point locations were assessed visually using the visible image where the yellow- and/or red-attack stage could be identified. These validation points were compared to the manually classified infestation areas reported by Crosby and others [16]. From these locations, precision, recall, overall accuracy, and the F1 score were calculated for the seven different classifications performed.

Table 2. Correlations between principal components and spectral reflectance bands of the original WorldView-2 image.

		Principal Component							
		1	**2**	**3**	**4**	**5**	**6**	**7**	**8**
Bands	**1**	0.455	−0.79	0.001	−0.146	−0.32	−0.126	0.165	0.048
	2	0.494	−0.817	−0.014	−0.141	−0.227	−0.058	−0.116	−0.03
	3	0.671	−0.716	−0.084	−0.021	−0.063	0.16	0.003	0.034
	4	0.581	−0.805	0.022	−0.04	0.066	0.006	0.012	−0.024
	5	0.494	−0.847	0.05	−0.098	0.146	−0.049	−0.014	0.049
	6	0.969	−0.175	−0.029	0.174	−0.007	−0.014	0.002	0.002
	7	0.982	0.133	−0.125	−0.047	0.01	−0.005	0.001	−0.001
	8	0.988	0.109	0.105	−0.02	−0.005	0.005	<0.001	<0.001

3. Results

The unsupervised classification utilizing all reflectance bands yielded a classification that shows 3100 hectares being actively infested by SPB which was greater than three times the area of active infestation. The classification using all bands produced an F1 score of 58.5% (Table 3). Classified areas of active infestation are distributed throughout the forest, but there are multiple areas of obvious misclassification (Figure 2a). The area of active infestation is far less in the classification of only the visible bands (i.e., bands 1–5; Figure 2b) which also had the greatest F1 score of all the classifications of spectral bands (88.6%). Classification results using bands 6–8 (Figure 2c) and 2, 4, and 5 (Figure 2d) were inaccurate in both area and F1 scores.

Table 3. Precision, recall, accuracy, F1 score, and acreages for each image/combination classified. The classifications include object classification of a combination of PC 1 and 2 (PC12OBJ), PC1 alone (PC1OBJ), and PC2 alone (PC2OBJ). The remaining classifications compared were all spectral bands (all bands), and those most correlated with PC 1 and/or PC 2 (bands 1–5, bands 6–8, and bands 2, 4, and 5).

	Image						
	PC12OBJ	*PC1OBJ*	*PC2OBJ*	*All Bands*	*Bands 1–5*	*Bands 6–8*	*Bands 2, 4, 5*
Precision	81.3	13.3	56	41.3	82.3	30.7	45.3
Recall	100	90.9	97.7	100	95.4	95.8	89.5
Accuracy	90.7	56	77.3	70.7	89.3	64.7	70
F1	89.7	23.3	71.2	58.5	88.6	46.5	60.2
Acreage	1527.7	5066.7	965.8	3100.1	1271.4	3474.6	1550.7

Open areas, forest edges, and rights-of-ways had multiple spots incorrectly classified as active infestation. Additionally, there were single pixels sporadically occurring throughout the image (e.g., a salt-and-pepper effect). Showing a classified location in detail, compared to the visible image of an infested location that has been partially treated (Figure 3a–e), the misclassification is evident. Bands 6–8 (Figure 3b) show pixels and small groupings throughout the area, while the classification performed on bands 2, 4, and 5 (Figure 3c) shows the treated area as infested more clearly than the area to the east that is infested (i.e., the area of red in Figure 3a). All bands captured most of the infested and treated areas and show the salt-and-pepper effect throughout the adjacent healthy forest (Figure 3d). The classification of bands 1–5 (Figure 3e), while imperfect, captured a majority of the infested area and illustrates the edge of the treated area that is shown as infested.

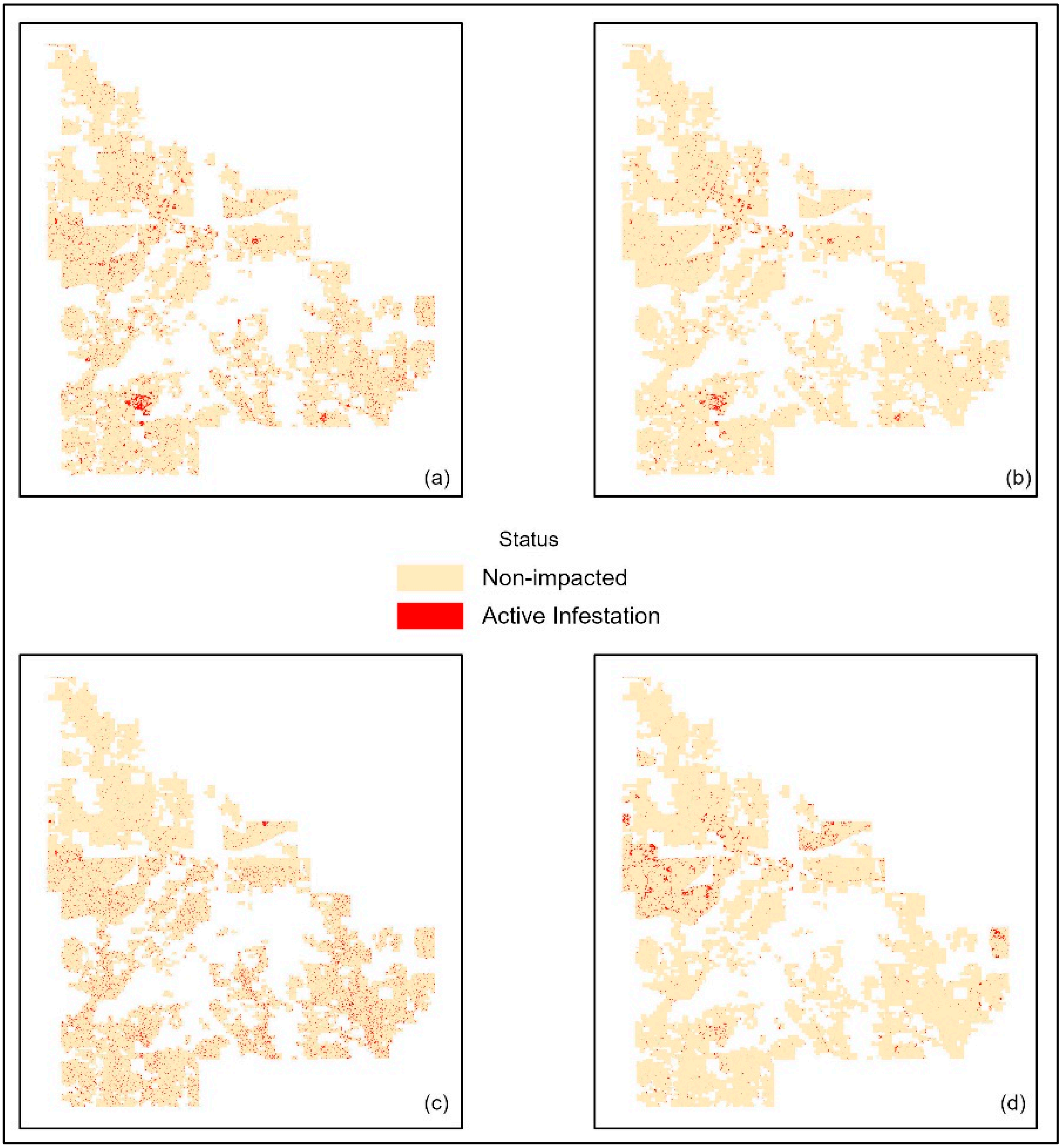

Figure 2. Unsupervised classification results for WorldView-2 image for (**a**) all spectral bands, (**b**) bands 1–5, (**c**) bands 6–8, and (**d**) bands 2, 4, and 5.

The principal components classified using three PC combinations show starkly different results compared to each other. The combination of PC_1 and PC_2 (Figure 4a; Table 3) had the greatest F1 score while PC_1 alone (Figure 4b) had the lowest F1 score and greatest area estimate of any combination classified with either method. Visually, the PC combinations are starkly different (Figure 5a,d). Assessing PC_1 alone (Figure 5b) showed many small objects identified as infestation adjacent to the treated area and infested spots (Figure 5a). PC_2 alone (Figure 5c) grossly underestimated the areas that are actively infested, which may be expected given the low variance found in the second PC (Table 1) and small area actively infested estimates from the classification (Table 3). The combination of PC_1 and PC_2 (Figure 5c) has a few spots along the forest/treated edge classified as infested. Compared to the three band combinations, the coverage of SPB infestations varied wildly throughout the forest depending upon which combination of PC/bands was classified (Figures 2a–d and 4a–c). The object classification using combined PC_1 and PC_2 provided the most accurate classification (assessed by F1 score; Figure 4a), though it was only marginally better than the classification using bands 1–5 (Figure 2b), which were most closely correlated with PC_2 (89.7% vs. 88.6%, respectively; Table 3). The area estimates are different, with PC_1 and PC_2 showing 1528 hectares and bands 1–5 showing 1271 hectares; both overestimated the area of active infestation (953 hectares; [16]) by 60 and 33%, respectively (Table 3). While bands 1–5 produced an area estimate closer to the accepted area, there were similar errors in the classification using all bands with misclassification in rights-of-ways. Combining PC_1 and PC_2 produced more contiguous areas of active infestation (Figure 5c, often covering the whole of an infested spot even though, visibly, some portions may appear non-infested. A few objects appear misclassified as actively infested along rights-of-ways (Figure 4a).

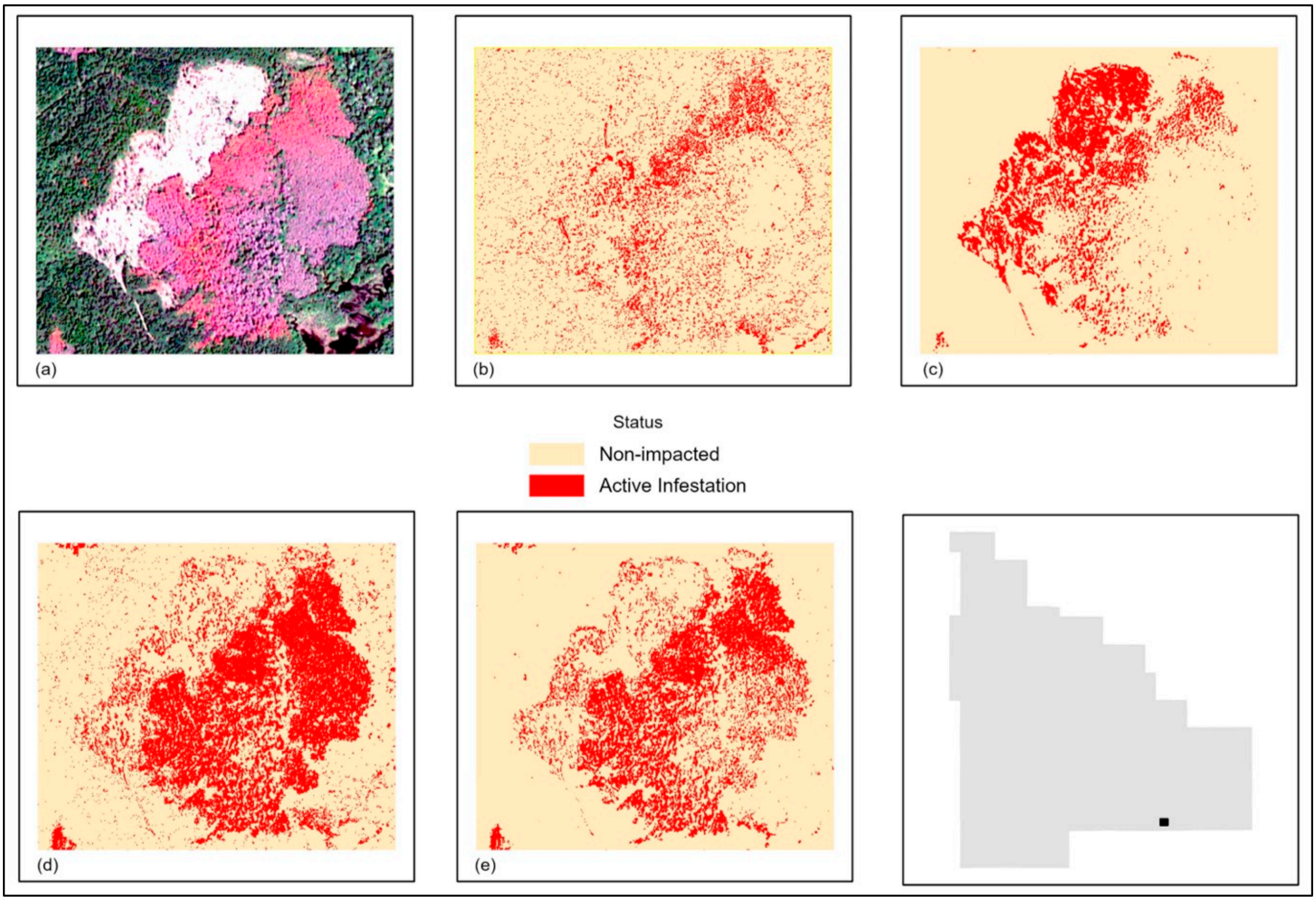

Figure 3. An area within the BNF showing multiple land cover types in a visible image (**a**), the unsupervised classification results for bands 6–8 (**b**), bands 2, 4, and 5 (**c**), all spectral bands (**d**), and bands 1–5 (**e**). The grayscale area is a reference where the location shows within the BNF.

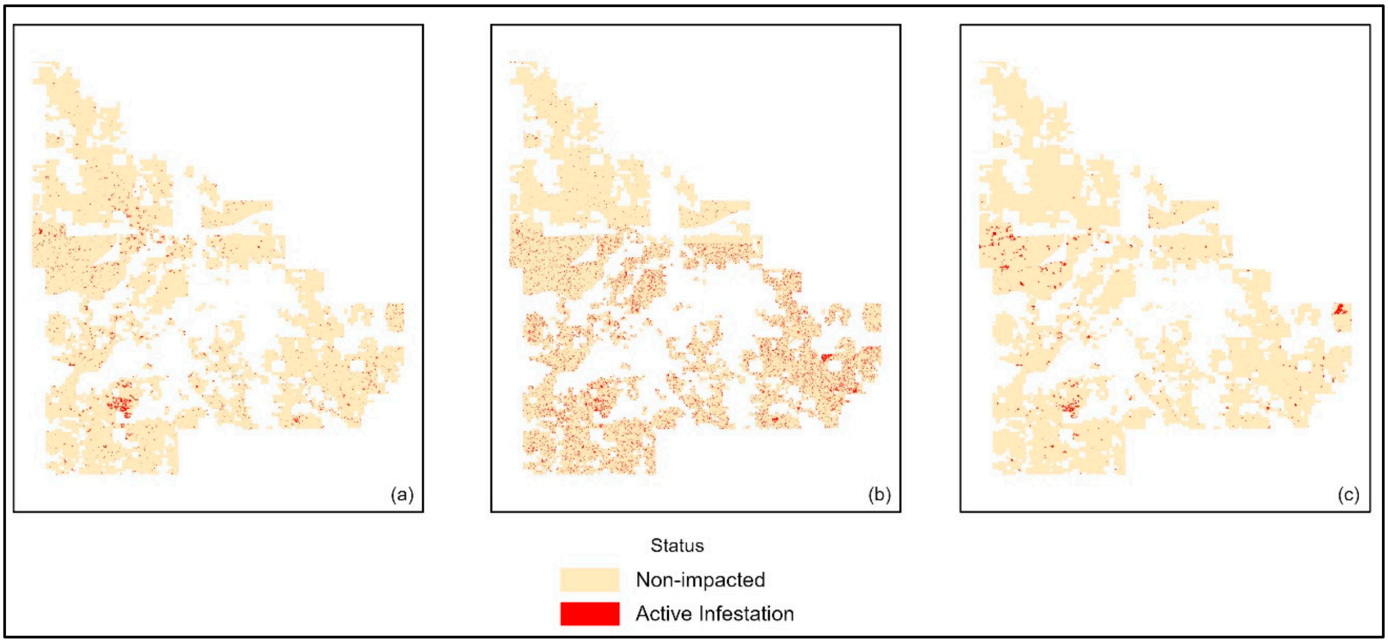

Figure 4. Unsupervised object classifications of (**a**) principal components 1 and 2, (**b**) principal component 1 alone, and (**c**) principal component 2 alone.

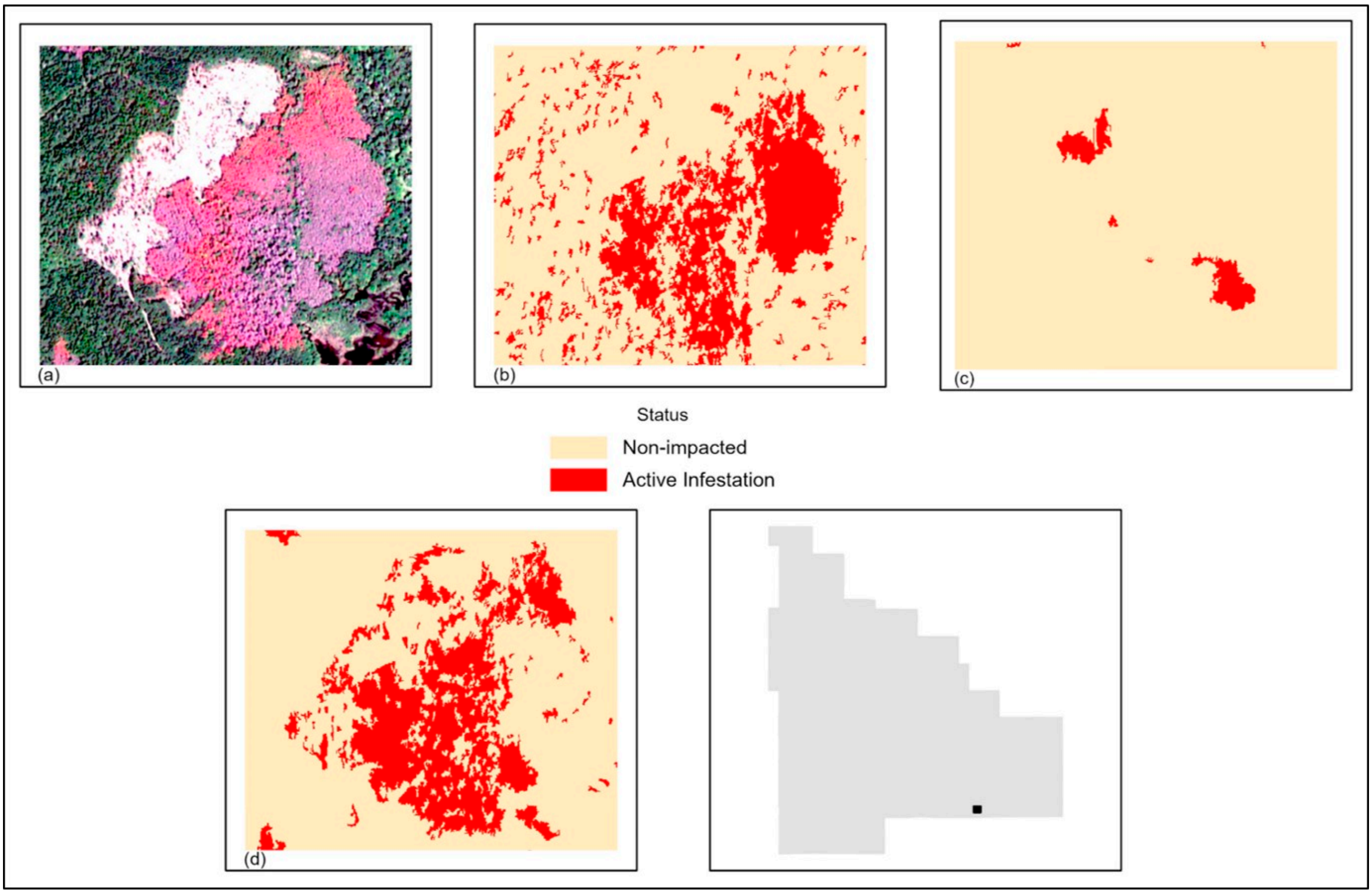

Figure 5. An enhanced area within the BNF showing a visible image (**a**) and the unsupervised object classification results of PC_1 alone (**b**), PC_2 alone (**c**), and the combination of PC_1 and PC_2 (**d**). The grayscale area is a reference where the location shows within the BNF.

Classifying PC_1 alone provided the lowest accuracy and the largest area estimate (Table 3). Objects classified with PC_1 alone are widely scattered with most of the areas classified as active infestation appearing to be shadows, rights-of-ways, and water (Figure 5b). Considering the classification of PC_2 alone, the third greatest accuracy was observed, and an area estimate was found that only slightly underestimated the area of active infestation; however, much of the area missed was an open area along an interstate highway. Some areas of water and open fields were misclassified as active infestation using PC_2 alone (Figure 4c). The other images classified (using red edge, NIR1, and NIR2 bands and blue, red, and yellow bands) did not produce great accuracies and overestimated area (Table 3). Edges near rights-of-ways and shadows were often misclassified, leading to a salt-and-pepper effect in the classified image (Figure 2b–d).

4. Discussion

Utilizing principal components provided a means of increasing the accuracy of classifying disturbance within the BNF due to SPB. Removing the noise added to classifications by unnecessary spectral data provides a means of more accurately representing conditions in the forest and provides forest managers a method of assessing areas of natural disturbance within a forest. Comparing the best PC and spectral band classifications (Figure 6a–c), the noise of classifying spectral bands versus PCs is evident. The object classification of PC results produces a smoother map (Figure 6c) and is less susceptible to individual pixels with small groups of pixels showing up throughout an image (Figure 6b) that would lead to a waste of field resources, sending people to physically check or treat locations where there is no infestation. Classifying the PCA results is a more efficient method than the manual interpretation of imagery (e.g., digitizing; [16]). The combined visible and NIR data led to too much variance in the image for accurate classification [28]. In this study, incorporating all spectral bands in an image provides too much noise in the classification, which leads to inaccuracies that the PCs help overcome [22,29]. Determining principal components is a relatively straightforward process that will allow analysts of any skill level to determine the most effective bands to use in determining disturbance agents or to use object classification of the PCs directly. Other locations and image sources would likely alter the PC results, in terms of the amount of variance accounted for with each successive PC. It is likely that the first two or three PCs would account for 90% or more of the variance. Using this methodology in another area would provide an interesting comparison of whether there is some threshold of cumulative variance in PCs that aids in classifying disturbance. It would also be interesting in future studies to determine if the principal components change with disturbance agents (SPB vs. EAB, drought, wind damage, etc.).

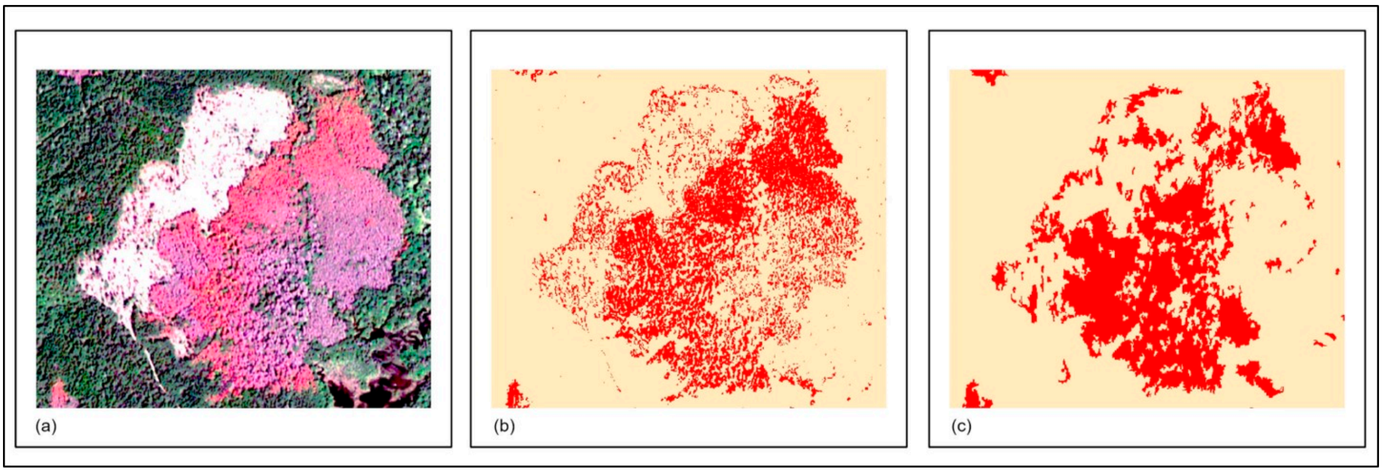

Figure 6. A comparison of a visible image showing an active area of SPB infestation (**a**), the classification results of bands 1–5 (**b**), and the object classification of PC_1 and PC_2 (**c**).

It was noteworthy that the image with the photosynthetically active radiation (PAR) detecting bands produced such a high accuracy classification. Typically, vegetation indices are used to identify plant stress [30]. Perhaps the inclusion of the yellow reflectance band provided enough spectral information to separate beetle-impacted trees. It has previously been found that the red edge is an important reflectance band for early detection [14]; however, the image that includes the red edge and the NIR reflectance bands did not produce as good a result. As the trees become more stressed and leaf stress starts to occur, there is a point at which the tree will appear spectrally as non-forest or standing dead, meaning the PAR/NIR detecting bands will not show the tree as actively infested. It may be useful to incorporate hyperspectral imagery [28] for such a task although this would increase cost for both acquisition of the imagery and processing time.

The spatial resolution of the imagery is important in detecting this shift as well as trees being attacked as the infestation spreads. Using a coarser resolution image, it may only be possible to detect plot or stand level damage, meaning that actively infested trees or the leading edge of an infestation may not be detectable [13,18]. Using imagery such as WorldView-2 allows for the detection of SPB infestation and can be used for a prompter response. While the combination of PC_1 and PC_2 provided the most accurate classification, the area of SPB infestation was overestimated. This could potentially be the result of the object classifier grouping spectrally similar pixels. The overprediction of acreage infested may result in visiting areas that do not have actively infested trees but would be better than missing infested areas that could lead to further spread in the forest. The visible bands (1–5), when classified, yielded a more conservative estimate of the area infested, but were still greater than the active acreage previously determined [16]. This could be explained by trees, or portions of trees that are actively infested, having enough photosynthesizing vegetation to not yet appear as being stressed. There could also potentially be reflectance being detected from understory vegetation mixing into the pixel.

The attack stage is an important consideration in early detection of infestation. Early stages of infestation—i.e., green—may spectrally favor green vegetation and lead to inaccurate classification. Abdullah and others [31] found that red-edge spectral data were beneficial in detecting green attacks in trees. This study did not directly assess the attack stage, but future research could address this using PCA and training data from plot-level surveys to build neural network models to classify vegetation threats [22,32]. Early identification of tree stress would allow for mitigating measures to be taken to prevent the further spread of SPB in a forest [11]. In this study, areas that have received some amount of treatment to mitigate further spread of SPB may have led to classification inaccuracies. One of the mitigation measures used on the BNF was cut-and-leave, where a buffer around impacted trees is cut and left in the forest. In some areas of the BNF, particularly with object classifications using principal components, it appears that some of these areas that were treated are detected as active infestation due to the similarly senescent vegetation of felled trees. Additional work would need to be done to incorporate temporally synchronized in situ measurements to better understand whether high-resolution imagery compensates for spectral similarities in treated vs. infested trees. Understory composition may also play a role in this and alternative methods such as spectral unmixing may also be considered. Masking areas of known treatment from imagery may be useful in avoiding overestimating the areas impacted.

It may be worthwhile to mask non-forest areas in imagery before performing classifications to assess forest disturbance. This is particularly true for high-resolution imagery where pixels appear in gaps in the canopy or spectral mixing occurs along edges that could be leading to misclassification. However, in an operational setting, this process may be time-consuming for a resource manager quickly attempting to determine where a disturbance is occurring. Altogether, the object classification of PC_1 and PC_2 was cleaner than that with visible bands, meaning there were fewer sporadic clusters from the segmented image and resulting objects compared to the salt-and-pepper effect in the spectral band classifications where single or few pixels will appear as actively infested throughout the classified image. This may be further refined with spectral and spatial relationships in the segmentation/classification.

The present study has the benefit of hindsight for identifying and verifying SPB spots over a large area. For periodic assessment of SPB activity, in practice, this methodology could be utilized with multi-temporal imagery. This imagery could be obtained and processed to identify potential hot spots and update risk maps for insect activity and/or to enhance efforts of modeling SPB behavior using machine techniques and projected climate change scenarios [24,33]. It may also be possible to obtain training data from high-resolution data, such as WorldView-2, and use it to classify regularly obtained imagery such as Sentinel or Landsat [18,34]. Given the spread of SPB further north [23], out of the southeastern United States, other regions will need to begin a means of assessing their presence and impacts on forested areas [7]. This could be a combination of field-based monitoring/trapping [6] and remotely sensed techniques like that covered here and with other sensors. Future research should consider forest density relationships with changes in spectral reflectance, particularly infrared portions of the spectrum commonly associated with healthy vegetation.

5. Conclusions

This study sought to accurately map insect disturbance using high-resolution remotely sensed data. Using PCA provides a way to more accurately map insect outbreaks. The improvements realized utilizing this method with high-resolution imagery will aid forest managers in more rapidly detecting SPB infestation and allocating resources to prevent further spread.

The result of using the visible bands was interesting and indicates that these bands may provide critical information for the assessment of insect disturbance. The unsupervised classification method used here was used to provide a relatively straightforward approach to determining SPB activity compared to healthy forests so that accurate information can be provided to decision-makers regarding treatment and mitigation protocols. The methods used in this study can be utilized with data from other sensors as well as hyperspectral data. Regardless of the data source, a readily available method of monitoring forests is necessary to form a proactive rather than reactive response to similar events in the future.

Author Contributions: Conceptualization, M.K.C., T.E.M. and J.J.H.; methodology, M.K.C.; writing—original draft preparation, M.K.C., T.E.M., J.J.H., J.R.M., C.A.S., B.L.S. and C.J.; writing—review and editing, M.K.C., T.E.M., J.J.H., J.R.M., C.A.S., B.L.S. and C.J.; funding acquisition, M.K.C., T.E.M. and J.J.H. All authors have read and agreed to the published version of the manuscript.

Funding: This research was funded by the U.S. Forest Service, Forest Health Protection Office in Pineville, LA (Grant Agreement 19-DG-11083150-025).

Data Availability Statement: Requests for data access can be made through the corresponding author.

Conflicts of Interest: The authors declare no conflict of interest.

References

1. Hanson, C.; Yonavjak, L.; Clarke, C.; Minnemeyer, S.; Boisrobert, L.; Leach, A.; Schleeweis, K. *Southern Forests for the Future*; World Resources Institute: Washington, DC, USA, 2010; p. 88. Available online: https://www.wri.org/research/southern-forests-future (accessed on 15 December 2023).
2. Oswalt, S.N.; Smith, W.B.; Miles, P.D.; Pugh, S.A. *Forest Resources of the United States, 2017: A Technical Document Supporting the Forest Service 2020 RPA Assessment*; Gen. Tech. Rep. WO-97; Department of Agriculture, Forest Service, Washington Office: Washington, DC, USA, 2019; p. 223. [CrossRef]
3. Winn, M.F.; Gray, J.A.; Cooper, J.A.; Bentley, J.W. *Southern Pulpwood Production, 2020. Resource Bulletin SRS–234*; Department of Agriculture Forest Service, Southern Research Station: Asheville, NC, USA, 2022; p. 13. [CrossRef]
4. Pye, J.M.; Holmes, T.P.; Prestemon, J.P.; Wear, D.N. *Economic Impacts of the Southern Pine Beetle*; Coulson, R.N., Klepzig, K.D., Eds.; Southern Pine Beetle II. Gen. Tech. Rep. SRS-140; Department of Agriculture Forest Service, Southern Research Station: Asheville, NC, USA, 2011; pp. 213–222. Available online: https://www.srs.fs.usda.gov/pubs/gtr/gtr_srs140/gtr_srs140_213.pdf (accessed on 14 December 2023).

5. Nowak, J.T.; Meeker, J.R.; Coyle, D.R.; Steiner, C.A.; Brownie, C. Southern Pine Beetle infestation in relation to forest stand conditions, previous thinning, and prescribed burning: Evaluation of the Southern Pine Beetle Prevention Program. *J. For.* **2015**, *113*, 454–462. [CrossRef]
6. Sullivan, B.T.; Munro, H.L.; Shepherd, W.P.; Gandhi, J.J.K. 4-allylanisole as a lure adjuvant for *Dendroctonus frontalis* (Coleoptera: Curculionidae: Scolytinae) and two associated beetles. *J. Appl. Entomol.* **2022**, *146*, 813–822. [CrossRef]
7. McNichol, B.H.; Sullivan, B.T.; Munro, H.L.; Montes, C.R.; Nowak, J.T.; Villari, C.; Gandhi, K.J.K. Density dependent variability in an eruptive bark beetle and its value in predicting outbreaks. *Ecosphere* **2021**, *12*, e03336. [CrossRef]
8. Clarke, S.R.; Meeker, J.R.; Dodds, K.J. Revised and potential new tactics for the suppression of Southern Pine Beetle Infestations. *J. Integr. Pest Manag.* **2021**, *12*, 35. [CrossRef]
9. Carter, G.A.; Seal, M.R.; Haley, T. Airborne detection of southern pine beetle damage using key spectral bands. *Can. J. For. Res.* **1998**, *28*, 1040–1045. [CrossRef]
10. Meddens, A.J.H.; Hicke, J.A.; Vierling, L.A.; Hudak, A.T. Evaluating method to detect bark beetle-caused tree mortality using single-date and multi-date Landsat imagery. *Remote Sens. Environ.* **2013**, *132*, 49–58. [CrossRef]
11. Immitzer, M.; Atzberger, C. Early detection of bark beetle infestation Norway spruce (*Picea abies*, L.) using WorldView-2 data. *Photogramm. Fernerkund. Geoinf.* **2014**, *5*, 351–367. [CrossRef]
12. Bright, B.C.; Hudak, A.T.; Egan, J.M.; Jorgensen, C.L.; Rex, F.E.; Hicke, J.A.; Meddens, A.J.H. Using satellite imagery to evaluate beetle-caused tree mortality reported in aerial surveys in a mixed conifer forest in northern Idaho, USA. *Forests* **2020**, *11*, 529. [CrossRef]
13. Gomez, D.F.; Ritger, H.M.W.; Pearce, C.; Eickwort, J.; Huler, J. Ability of remote sensing systems to detect bark beetle spots in the southeastern US. *Forests* **2020**, *11*, 1167. [CrossRef]
14. Abdullah, H.; Darvishzadeh, R.; Skidmore, A.K.; Heurich, M. Sensitivity of Landsat-8 OLI and TIRS data to foliar properties of early stage bark beetle (*Ips typographus*, L.) infestation. *Remote Sens.* **2019**, *11*, 398. [CrossRef]
15. Waser, L.T.; Küchler, M.; Jütte, K.; Stampfer, T. Evaluating the potential of WorldView-2 data to classify tree species and different levels of ash mortality. *Remote Sens.* **2014**, *6*, 4515–4545. [CrossRef]
16. Crosby, M.K.; McConnell, T.E.; Holderieath, J.J.; Meeker, J.R.; Steiner, C.A.; Strom, B.L.; Johnson, C.W. Tracking the extent and impacts of a Southern Pine Beetle (*Dendroctonus frontalis*) outbreak in the Bienville National Forest. *Forests* **2023**, *14*, 22. [CrossRef]
17. Senf, C.; Seidl, R.; Hostert, P. Remote sensing of forest insect disturbances: Current state and future directions. *Int. J. Appl. Earth Obs. Geoinf.* **2017**, *60*, 49–60. [CrossRef]
18. Abdullah, H.; Skidmore, A.K.; Darvishzadeh, R.; Heurich, M. Sentinel-2 accurately maps green-attack stage of European spruce bark beetle (*Ips typographus*, L.) compared with Landsat-8. *Remote Sens. Ecol. Conserv.* **2019**, *5*, 87–106. [CrossRef]
19. Hicke, J.A.; Logan, J. Mapping whitebark pine mortality caused by a mountain pine beetle outbreak with high spatial resolution satellite imagery. *Int. J. Remote Sens.* **2009**, *30*, 4427–4441. [CrossRef]
20. Dash, J.P.; Watt, M.S.; Pearse, G.D.; Heaphy, M.; Dungey, H.S. Assessing very high resolution UAV imagery for monitoring forest health during a simulated disease outbreak. *ISPRS J. Photogramm. Remote Sens.* **2017**, *131*, 1–14. [CrossRef]
21. Byrne, G.F.; Crapper, P.F.; Mayo, K.K. Monitoring land-cover change by principal component analysis of multitemporal Landsat data. *Remote Sens. Environ.* **1980**, *10*, 175–184. [CrossRef]
22. Eeti, L.N.; Buddhiraju, K.M.; Bhattachary, A. A single classifier using principal components vs. multi-classifier system: In Landuse-LandCover Classification of WorldView-2 Sensor Data. *ISPRS Ann. Photogramm. Remote Sens. Spat. Inf. Sci.* **2014**, *2*, 91–95. [CrossRef]
23. Dodds, K.J.; Aoki, C.F.; Arango-Velez, A.; Cancelliere, J.; D'Amato, A.W.; DiGirolomo, M.F.; Rabaglia, R.J. Expansion of southern pine beetle into northeastern forests: Management and impact of a primary bark beetle in a new region. *J. For.* **2018**, *116*, 178–191. [CrossRef]
24. Munro, H.L.; Montes, C.R.; Gandhi, K.J.K. A new approach to evaluate the risk of bark beetle outbreaks using multi-step machine learning methods. *For. Ecol. Manag.* **2022**, *520*, 120347. [CrossRef]
25. Hexagon Geospatial. ERDAS Imagine 2018 Release Guide. 2018. Available online: https://bynder.hexagon.com/m/4c3e79ff5da8e015/original/Hexagon_GSP_ERDAS_IMAGINE_2018_Release_Guide.pdf (accessed on 20 July 2023).
26. Jensen, J.R. *Introductory Digital Image Processing: A Remote Sensing Perspective*, 3rd ed.; Prentice Hall: Upper Saddle River, NJ, USA, 2005; p. 526.
27. ESRI. *ArcGIS Pro, Version 2.8*; Environmental Systems Research Institute: Redlands, CA, USA, 2021.
28. Machidon, A.L.; Del Frate, F.; Picchiani, M.; Machidon, O.M.; Ogrutan, P.L. Geometrical approximated principal component analysis for hyperspectral image analysis. *Remote Sens.* **2020**, *12*, 1698. [CrossRef]
29. Arslan, N.; Nezhad, M.M.; Heydari, A.; Garcia, D.A.; Sylaios, G. A principal component analysis methodology of oil spill detection and monitoring using satellite remote sensing sensors. *Remote Sens.* **2023**, *15*, 1460. [CrossRef]
30. Assal, T.J.; Sibold, J.; Reich, R. Modeling a historical Mountain Pine Beetle outbreak using Landsat MSS and multiple lines of evidence. *Remote Sens. Environ.* **2014**, *155*, 275–288. [CrossRef]
31. Abdullah, H.; Skidmore, A.K.; Darvishzadeh, R.; Heurich, M. Timing of red-edge and shortwave infrared reflectance critical for early stress detection induced by bark beetle (*Ips typographus*, L.) attack. *Int. J. Appl. Earth Obs. Geoinf.* **2019**, *82*, 101900. [CrossRef]
32. Xia, B.; Kong, F.; Zhou, J.; Wu, X.; Xie, Q. Land resource use classification using deep learning in ecological remote sensing images. *Comput. Intell. Neurosci.* **2022**, *2022*, 7179477. [CrossRef] [PubMed]

33. Munro, H.L.; Montes, C.R.; Kinane, S.M.; Gandhi, K.J.K. Through space and time: Predicting numbers of an eruptive pine tree pest and its predator under changing climate conditions. *For. Ecol. Manag.* **2021**, *483*, 118770. [CrossRef]
34. Hart, S.J.; Veblen, T.T. Detection of spruce beetle-induced tree mortality using high- and medium-resolution remotely sensed imagery. *Remote Sens. Environ.* **2015**, *168*, 134–145. [CrossRef]